Analyst

Characterization of the Impact of Mixing and Droplet Volumes on the Behavior of Microfluidic Ion-Selective Droptodes

Journal:	*Analyst*
Manuscript ID	AN-ART-04-2021-000733.R1
Article Type:	Paper
Date Submitted by the Author:	22-Jun-2021
Complete List of Authors:	Wetzler, Shannon; University of Michigan, Chemistry Meyerhoff, Mark; University of Michigan, Chemistry Bailey, Ryan; University of Michigan, Department of Chemistry

ARTICLE

Characterization of the Impact of Mixing and Droplet Volumes on the Behavior of Microfluidic Ion-Selective Droptodes

Received 00th January 20xx,
Accepted 00th January 20xx

DOI: 10.1039/x0xx00000x

Shannon P. Wetzler-Quevedo, Mark E. Meyerhoff, and Ryan C. Bailey*

Droplet microfluidic optodes, or "droptodes", have emerged as a powerful technology for rapid detection of small ions in complex matrices. While using segmented aqueous phases provides the benefits of sample isolation, the influence of the liquid nature of the oil carrier phase has not yet been explored. In this paper, we examine the influence of microfluidic parameters on droptode efficiency, using potassium-sensitive droptodes as a model system. We found that while changing flow rates on device does not change droptode performance, both channel geometry and droplet size significantly impact droptode efficiency. Specifically, enhanced mixing of the droplets leads to faster equilibration on device and lowers limits of detection by about one order of magnitude. We also found that increasing the size of the sample droplet, at the expense of the size of the oil carrier/sensing phase, leads to higher sensitivity in the linear region of the droptode. These easily manipulated properties will allow one device to potentially be adapted for several different applications, based upon the type and concentration range of measurement required.

Introduction

The rapid and sensitive detection of ions in a variety of matrices is critical not only for monitoring reaction progress and potential contamination, but also for disease diagnostics useful in clinical practice. Traditionally, ions are measured using ion-selective electrodes (ISEs) or ion-selective optodes (ISOs): technologies that exhibit a change in voltage or color/fluorescence, respectively, depending on the presence of an ion of interest.[1,2] ISOs offer the additional benefit of minimal instrumentation, leading to a high potential for ISOs as low-cost point-of-care devices.[2] Additionally, changes in organic phase composition and the ratio of organic and aqueous phases have been shown to affect optode sensitivity.[3] However, ISOs suffer from the need for milliliters of sample, equilibration times on the orders of minutes, and the possibility of leaching reagents into the sample. These limitations, along with swelling of the PVC or other polymeric matrices that typically comprise the optodes, greatly decrease ISOs' long-term usage and reliability for clinical practice.[2,4,5]

In response to these drawbacks, we have developed a droplet microfluidic optode system, which we have termed as "droptodes."[6] In a droptode system, the aqueous phase is segmented into individual micro- to nano-liter sized droplets separated by an immiscible carrier oil phase containing a chromoionophore, an ionophore with selectivity towards the analyte of interest, and an ion-exchanger. Ion-exchange takes place across the aqueous/oil boundary, leading to an ion-dependent change in the charge state of the chromoionophore causing a colorimetric and/or fluorometric signal change (Figure 1).

Droptode measurements are performed in only seconds, do not suffer from leaching of reagents, and use very small (nL-µL) sample sizes. Additionally, droptode channels are fabricated in poly(dimethylsiloxane) (PDMS)devices, which allow for low cost and rapid prototyping.[7] Droptode technology has been shown to be compatible with detection of cations, anions, and polycations, and can operate with complex sample matrices such as whole blood, owing to the fact that the optical signal measurement is made in the oil phase.[6]

While droptodes have opened up a novel means of analyzing ions using microfluidics, the benefits of droplet microfluidics on the droptode system have not yet been fully exploited. Droplet microfluidics allows for real-time analysis, modulation of droplet size and composition, and the varying of droplet speeds.[8-10] Thus, the flexibility of droplet microfluidics could allow for one droptode device to be used for measurement over a variety of concentration ranges by simply changing fluidic parameters.

Herein, the impacts of experimental parameters on droptode sensitivity using a potassium-sensitive droptode system are explored. Specifically, we analyzed the impact of droplet speed and position of measurement relative to droplet generation on droptode sensitivity. We found that, despite spending the same amount of time on device, changing droplet speed and the position of measurement on device do not lead to the same changes in sensitivity. However, we confirmed that channel-induced mixing leads to droptodes with increased

Department of Chemistry, University of Michigan, Ann Arbor, Michigan, 48109, United States. Phone: 734.764.1438. Email: ryancb@umich.edu

†Electronic Supplementary Information (ESI) available: See DOI: 10.1039/x0xx00000x

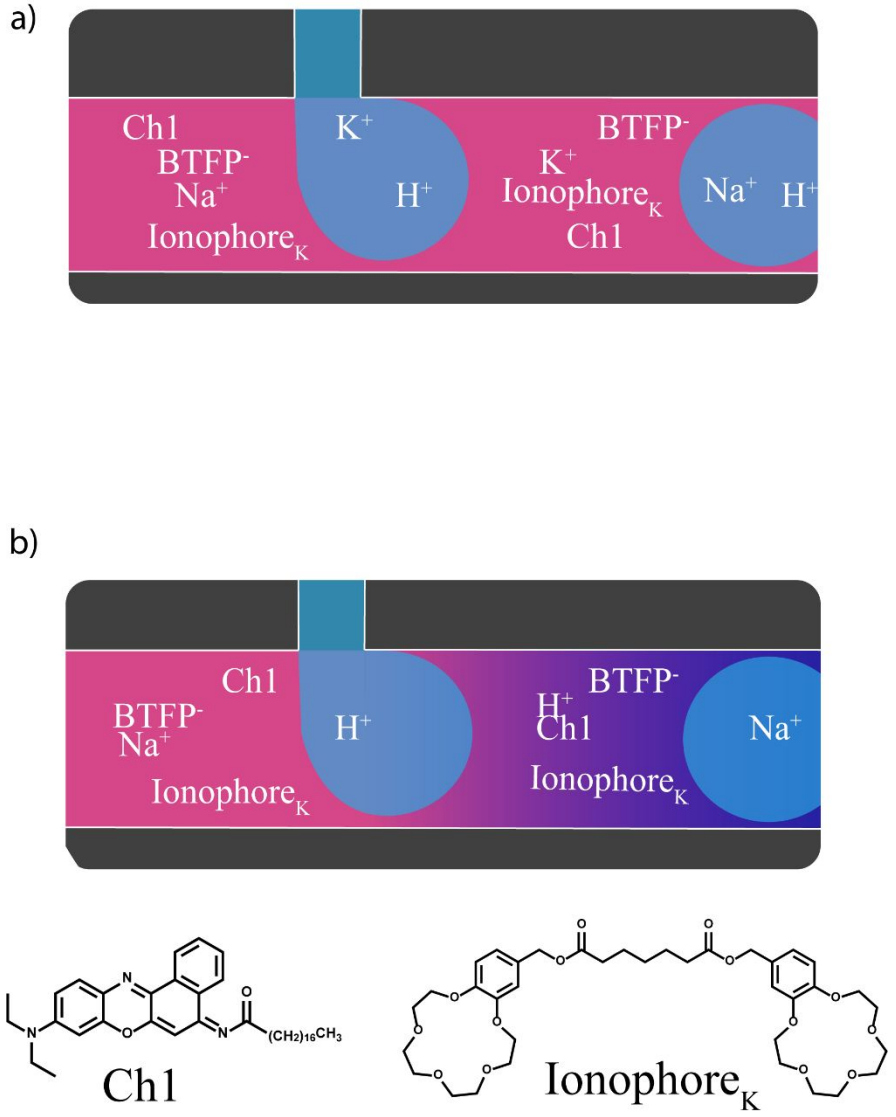

Figure 1. Mechanism for potassium detection in droptode. (a) When no potassium is present, a proton is used to balance the charge caused by the ion exchanger (NaBTFP), leading to a change in the chromophoric properties of the chromoionophore (Ch1). (b) When potassium is present, it bonds with the specific ionophore and transfers into the oil phase. The positive charge from potassium balances the negative charge from the ion exchanger, meaning no proton transfer is needed and there is no change in color and/or fluorescence.

sensitivity at low concentrations by almost an order of magnitude. We also analyzed the impact of changing droplet volume compared to carrier volume, finding that a higher aqueous volume provides a more sensitive linear region, but reduces the dynamic range at lower concentrations. Taken together, these studies support the fact that droptodes can be tuned to optimize analytical performance for diverse measurement applications.

Experimental Section

Chemicals and Materials

Unless otherwise stated, all chemicals were purchased from Sigma Aldrich. SU-8 2025 negative epoxy photoresist was a product of MicroChem Corp. Silicon wafers were purchased from University Wafer. Tridecafluoro-1,1,2,2-tetrahydrooctyl silane was from Gelest Inc. Poly(dimethylsiloxane) (PDMS) was purchased as separate base and curing agents from Momentive Performance Materials. 24-gauge needles and plastic syringes were obtained from Thermo Fisher Scientific. 24-gauge PTFE tubing was from Cole-Parmer. The syringe pumps used were Pump 11 Pico Plus Elite models from Harvard Apparatus.

Device Fabrication

Devices were fabricated using standard soft lithography techniques.[7] SU-8 2025 negative epoxy photoresist was applied to a clean Silicon wafer to a thickness of 40 µm via spin-coating. Masks were designed in AutoCAD software (Autodesk, Inc.) and were printed as transparencies (CAD/Art Services, Inc) for use in photolithography. After wafer baking and development, tridecafluoro-1,1,2,2-

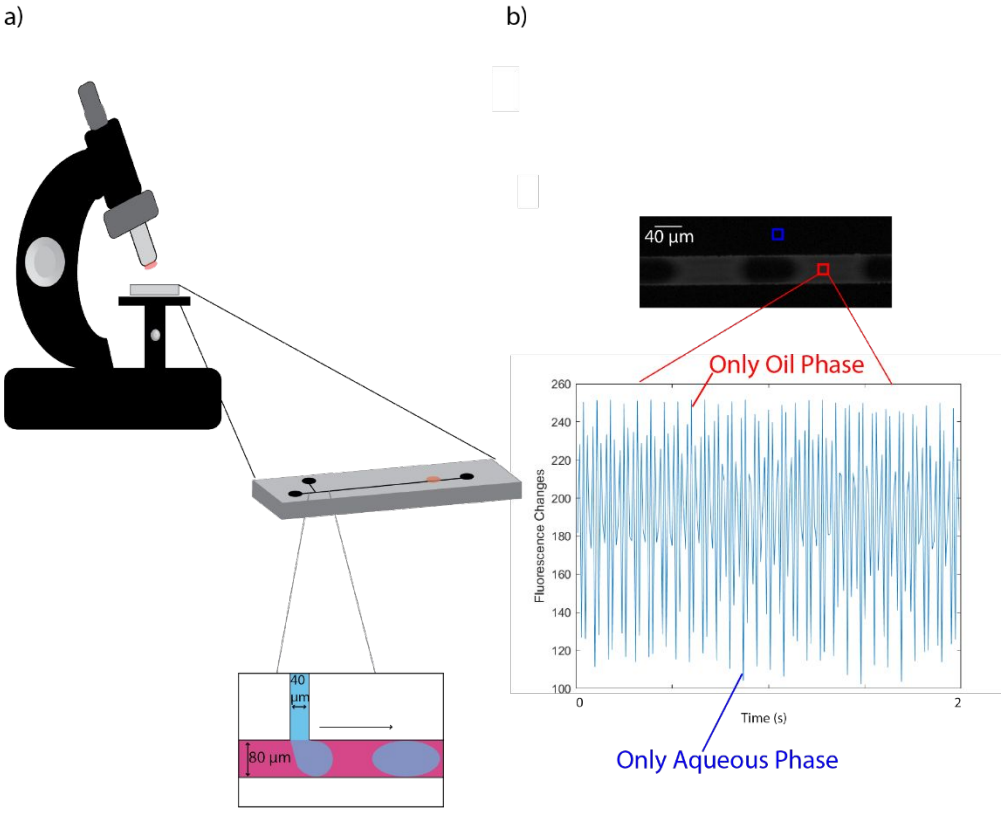

Figure 2. Method of droptode measurement. (a) Droplets were formed using a PDMS microfluidic device and their fluorescence was measured using a fluorescent microscope. (b) In order to track fluorescence, a set area within the channel as analyzed for its fluorescence changes. The background (blue box) from outside the channel was subtracted frame by frame. The maximums of the peaks represent where only the oil phase was analyzed. The minimums of the peaks represent where only the aqueous phase was analyzed. All points in between are analyses where both the oil and aqueous phase were in the analysis box. The resulting peaks were then averaged.

tetrahydrooctyltrichlorosilane was deposited on the resulting master molds using vacuum assisted chemical vapor deposition. Devices were made from their respective masters using a 10:1 degassed mixture of RTV615 base:curing agent ratio. Holes for the inlet and outlet were punched using a 24-gauge needle and then devices were adhered to a glass slide using oxygen plasma bonding. All channels were 40 µm in depth and 80 µm in width, except for the aqueous inlet which was 40 µm in width (Figure 2a). The standard fluorescence measurement point was 3 cm from the T-junction unless otherwise noted.

Droptode Experiments

Samples were serially diluted from a 1 M potassium chloride (KCl) solution in pH 7.4 HEPES buffer. Stock solutions of 400 µM Chromoionophore I in dioctyl sebacate (DOS), 1 mM potassium Ionophore II in DOS, and 1 mM sodium tetrakis[3,5-bis(trifluoromethyl)phenyl] borate (NaTFPB) in DOS were aliquoted and stored at -20°C for up to three months. These stocks were used to make an oil phase with the final concentrations of 100 µM Chromoionophore 1, 300 µM potassium ionophore II, and 200 µM NaTFPB. Both the sample and oil solutions were loaded into plastic 3 mL syringes and flowed through 24-gauge PTFE tubing into the microfluidic device using syringe pumps to generate droplets. Unless otherwise noted, the solution delivery rate was 2 µL/min. The intensity of fluorescence at various points was determined using a Nile Red filter cube (Leica Microsystems), and a VEO 640L high speed camera (Vision Research Inc.) connected to a DMi8 light microscope (Leica Microsystems). The exposure time was set to 9900 µs with a gain of 2 and the sample rate was set to 100 pictures per second (pps).

Data Analysis

All images from a single calibration curve were analyzed as a single video in ImageJ (NIH). Droplet size, spacing and frequency were determined from brightfield images. For fluorescent images, the combined images were enhanced in their contrast to 0.3% saturation, and normalized using ImageJ software, for easier visualization. The fluorescence intensity within a 30 x 30-pixel spot in the middle of the channel was determined using ImageJ for each frame of the combined video samples, averaging about 40 measurements from oil segments. A separate measurement of the background was taken and subtracted from the in-channel fluorescence intensity on a frame-by-frame basis. The resulting measurements were then analyzed for peaks using MATLAB (Figure 2b, code in SI). To account for variations in light source and oil concentration, data were normalized (Equation 1):

$$Normalized\ Fluorescence = 1 - \frac{F - F_{Max}}{F_{Max} - F_{Min}} = 1 - \frac{F - F_{Buffer}}{F_{Buffer} - F_{2M}}\ [1]$$

where F is the fluorescence intensity from the sample, F_{2M} is the fluorescence intensity from a 2 M KCl solution in pH 7.4 0.1M HEPES as the aqueous phase, and F_{Buffer} is the fluorescence caused by the HEPES buffer only as the aqueous phase.

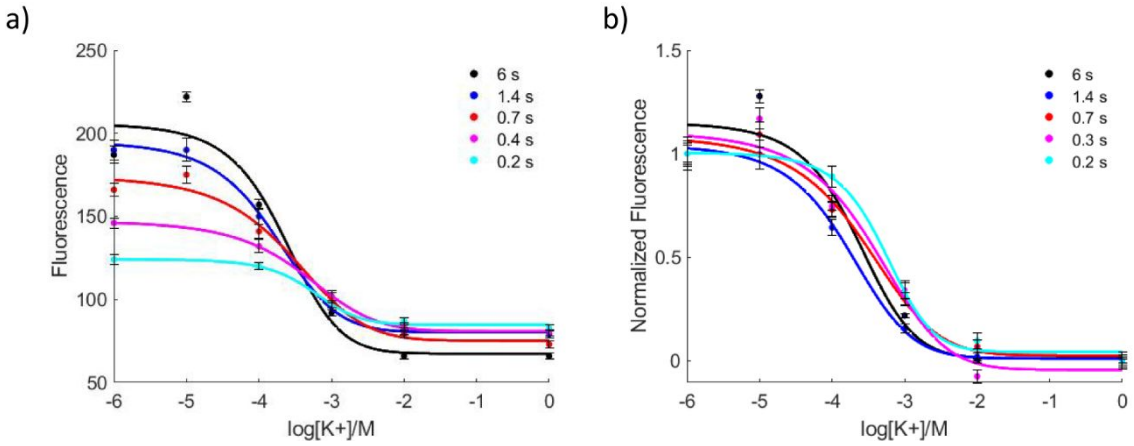

Figure 3. Fluorescence Measurements of potassium droptodes at various flow rates. (a) The original fluorescent measurements. Note that the maximum and minimum fluorescence is impacted by time on device. (b) The fluorescence normalized to the maximum and minimum fluorescence, defined by the buffer response and the response to 2M KCl, respectively. All except the fastest droptode, 0.2 s on device, have limits of detection within approximately 1 x 10^{-5} M of each other. Error bars represent the standard deviation between measurements (n=3).

The results of the measurements were then fit to a logistic curve against the log of the concentration of potassium to determine the limit of detection, the linear range, and the sensitivity of the various droptode conditions (Figure 3). The limit of detection (LoD) was calculated as the concentration at which

$$Signal = Signal_{Blank} - 3\sigma_{Blank}$$

That is to say, the concentration at which the signal is the same as the blank signal minus 3 times the noise in the baseline response, all after normalization. The negative value of the error was chosen due to the negative slope of the linear portion of the sigmoidal curve. Sensitivity was reported based on the slope found in the linear range of the fluorescence vs log concentration plot. Thus, sensitivity specifically refers to linear range sensitivity throughout this manuscript.

Results and Discussion

Initially, time on device was varied by changing the speed of droplet generation on the device. The ratio between the aqueous and oil flow rate remained equal, thereby keeping the size and spacing of the droplets consistent (SD: 4.3%), while the total flow rate was varied between 1 µL/min and 32 µL/min (SI Table 1). The resulting fluorescence curves (Figure 3a) demonstrate that a slower overall flow rate, and therefore more time on device, leads to greater fluorescence difference between the buffer and the 1 M potassium sample.

Once the curves were normalized using Equation 1 (Figure 3b), the curves appear to be similar in shape. The fastest moving droptode has a limit of detection of 2 x 10^{-4} M, about three times higher than all other speeds of droptodes tested, which converged at around 6 x 10^{-5} ± 2 x 10^{-5} M (Table S1). The convergence of limits of detection suggests that the majority of the droptode condition tested here achieved equilibrium between the two phases, with the exception of the fastest droplet generation rate.

Selectivity was minimally impacted by the droptode speed across a range of concentrations of the interfering ion (in this case sodium ions). The exception for this is when moving at the fastest droptode speed studied, where each droplet takes 0.2 s to traverse the length of the device to the detector. At that point, we see a decline in selectivity against both 0.1 M and 1 M NaCl, but not a selectivity decline against 1 x 10^{-3} M NaCl (Figure S1).

However, it is possible that changing the speed of the droplets, rather than just varying the time on device, also altered the speed of mixing by changing the velocity of local flow fields.[11] In order to test this, we analyzed the response of droptodes at

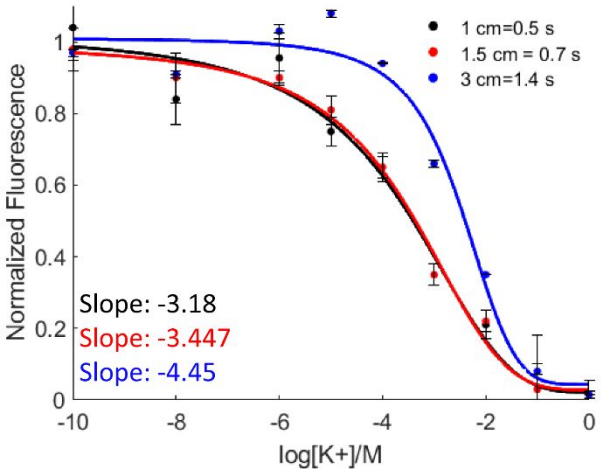

Figure 4. The impact of time on device by changing the measurement point on droptode behavior. The error bars are the standard deviation between measurements (n=3). As the droptode measurement point moved further from the T junction, the steeper and narrower the linear response range.

different distances from the droplet generation T-junction. If the only thing impacting the calibration curves was equilibration time, we would expect changing the droptode measurement position to result in similar calibration curves to those in Figure 3. However, as Figure 4 demonstrates, the calibration curves do not all converge. Specifically, the less time on device, based on measurement position, the lower limit of detection for the testing application. By spending half the amount of time on device, the limit of detection decreased from 5 x 10^{-5} M to 1.7 x 10^{-7} M (Table S2). This decrease in limit of detection was accompanied by a 1.3x reduction in the linear region. The dynamic range was increased, but sensitivity within the dynamic range was decreased by 33%. While these results seem counterintuitive, as more time on device should allow more time for equilibration, they were observed over three replicates and three different devices. Potential causes for this observed lower detection limit, such as PDMS leeching or competition between pH and potassium equilibration, will be the focus of future studies.

It is interesting to note that the calibration curves in Figure 4 do not exactly resemble those in Figure 3. This suggests that time for equilibration between the two phases is not the only factor that determines the magnitude of analyte response. Since all other conditions (such as droplet size, oil size, and device pattern) were held constant, the differences between Figures 3 and 4 suggest that mixing, which has been shown to change with changing flow rates,[11] could be one cause of this discrepancy.

It is also important to note that the change in position of measurement on device also impacted the selectivity of the device against sodium ions, but in this case the impact of the selectivity was more universal. The selectivity at an earlier point of detection was decreased for sodium concentrations ranging from 1 x 10^{-3} M to 1 M NaCl, which is an expanded range compared to that seen for changing total flow rate on device (Figure S2).

Impact of Mixing Devices

To determine if mixing would lead to improved sensitivity, we analyzed the behavior of potassium droptodes on a traditional mixing device. The serpentine curves in the mixing device are known to cause changes in the internal vortices within a droplet, allowing analytes previously stuck at the center of the droplets to come to the surface and have the potential to transfer more efficiently into the oil phase (Figure 5a).[11-14] In order to do a proper comparison between mixing and non-mixing channels, the position of measurement was kept consistent on both devices for calibration (1.5 cm and 3 cm from the junction, Figures 5c and 5d respectively).

For the serpentine device, it is important to clarify that the 3 cm point was mid-way through the device (Figure 5b) rather than being an endpoint of the device. The location was chosen

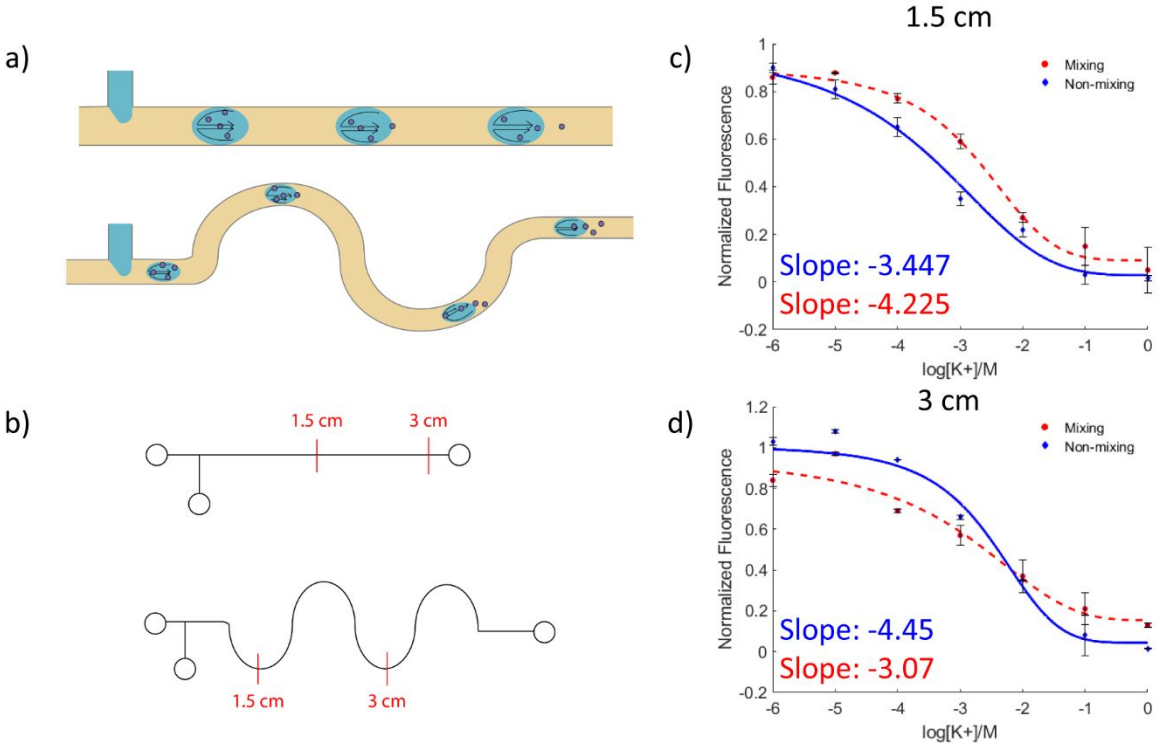

Figure 5.. Testing mixing microfluidic devices. (a) Adding serpentine channels promotes mixing within the droplet compared to straight channels. (b) Image of the T channel and serpentine device used for analysis with measurement locations marked. (c)Comparing droptode response between mixing and non-mixing device at 1.5 cm from the T junction. Notice that the non-mixing and mixing devices have different droptode responses, where the mixing device has a response very similar to the 3 cm response of the non-mixing device. (d) Droptode response between mixing and non-mixing device at 3 cm from the T junction. Notice that the mixing device, while less sensitive in the linear range, has an expanded linear range and a lower limit of detection. The error bars for all are based on standard deviation in measurements (n=3).

to ensure that the same time was spent on both the enhanced mixing and straight devices.

At 1.5 cm post-droplet generation, the non-mixing device appears to maintain a wider linear range and lower limit of detection. However, the response at 1.5 cm on the mixing device, looks similar to the response at 3 cm on the non-mixing device, with a limit of detection differing by 0.01 log units or 1 x 10^{-6} M (Figure S3). This suggests that the droptodes at 1.5 cm on the mixing device has achieved the same level of equilibrium as the droptodes at 3 cm on the non-mixing device. Thus, mixing appears to increase the speed to reach equilibrium between the oil and aqueous phases, and thus overall kinetics of K^+ response. While recording fluorescence at the 3 cm mark on the mixing device, by comparison, the LoD of the device is about an order of magnitude lower compared to the non-mixing device (9.5 x 10^{-6} M vs 4.4 x 10^{-5} M) (Table S3). From Figure 3 it appears that the non-mixing device equilibrates at these flow rates, while the mixing device does not. While the reason for this phenomena is unclear, it is possible that the additional mixing provided in the mixing device has caused the droptodes to enter the exhaustive sensing regime, lowering limits of detection but limiting sensitivity over a wider concentration range.

Droplet Volume Changes

One of the major advantages of using microfluidic droptodes is the fluidity of the oil phase. Rather than plasticizing a solid polymer to make it fluid-like, the liquid oil phase used in droptodes allows rapid transition in composition and size. Droplet microfluidics are known for their ability to form droplets of various sizes and spacing. Because optodes are known to have varying responses based on the ratios of their aqueous and organic phases,[2] we hypothesized that droplet size and spacing would similarly impact on droptode operation.

An important caveat to note is the lack of surfactants in this droptode system. Surfactants, most commonly used in microfluidics to stabilize droplets along their interfaces, have been shown to interfere with the operation of ion-selective electrodes.[15] Though no study has yet been performed as to the impact of surfactants on droptode behavior, surfactants were not used in our droptode system. Notably, the lack of surfactants does, at this stage, impact droplet size stability.

Using syringe pumps to control flow, the size and spacing of the droplets were inversely related. In order to keep the same total flow rate, as the aqueous flow rate was increased, the oil flow rate was decreased. For clarity, all flow conditions are reported as the ratio of the oil phase flow rate to the overall flow rate. A ratio of <0.5 is therefore a condition where the oil phase flow rate is less than the aqueous phase flow rate, and a ratio of >0.5 is where the oil phase flow rate is greater than the aqueous phase flow rate. A ratio of 0.5 means the oil phase flow rate and aqueous phase flow rate are equivalent. It was observed that as the aqueous flow rate increased, at the expense of the oil flow rate, the droplet size increased and the droplet spacing decreased. Similarly, a decrease in the aqueous flow rate, and increase in the oil flow rate, led to smaller droplets and larger droplet spacing (Figure 6a).

Three different flow rate ratios were used to study the impact of droplet sizing and spacing on the potassium calibration curve, with a total overall flow rate of 4 µL/min maintained throughout these experiments (Figure 6a and 6b). The higher error in these experiments is likely due to lack of droplet size stabilization when not using a 1:1 ratio of flows. As the size of the aqueous droplets increase and the size of the oil spacing decreases, the sensitivity of the droptode in the linear region also increases. Between the highest and lowest aqueous flow rates, there is an increase in the sensitivity by a factor of 2, and we also see an increase between the middle and lowest aqueous flow rates (Table S4). We hypothesize that the

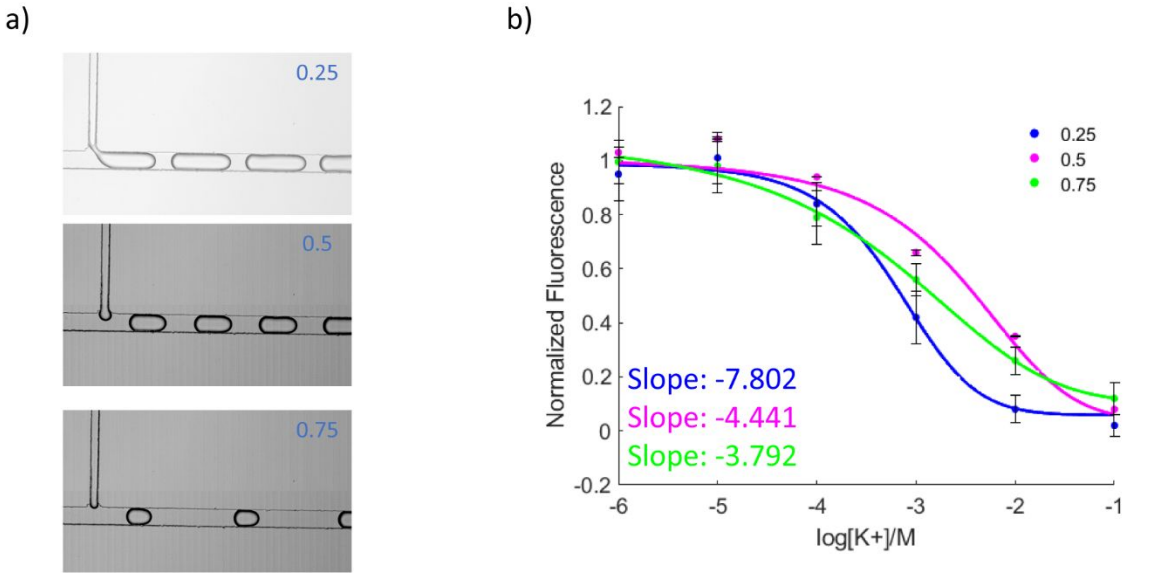

Figure 6. Droptode Performance with Changing Droplet Size. (a) The three different droplet conditions: 0.25 is 1 µL/min oil, 3 µL/min aqueous; 0.5 is 2 µL/min oil and 2 µL/min aqueous; 0.75 is 3 µL/min oil, 1 µL/min aqueous. (b) The results of running the potassium droptode under these conditions. The error bars are the standard deviation between measurements (n=3).

smaller oil phase leads to faster saturation of the chromoionophore in the oil phase, which leads to higher sensitivity.

However, the increase in sensitivity at high aqueous flow rates comes at the cost of the linear range. The linear range at high aqueous flow rates is a full order of magnitude smaller than at low aqueous flow rates (Figure 6b). Specifically, the linear range was increased to lower concentrations of potassium, all the way to 1 x 10^{-5} M K^+, compared to when the droplets were at their largest. There was about half an order of magnitude expansion of the linear range to higher concentrations of potassium as well in the largest oil spacing/smaller droplet size experiments. This increase in linear range at the largest oil spacing could potentially be caused again by the relative number of chromoionophore molecules in the oil droplet (fixed chromoionophore concentration)—particularly if operating in an exhaustive sensing regime. If there are more chromoionophore molecules, saturation will occur at higher higher analyte concentration (greater number of analyte molecules/volume), increasing the linear range at higher concentrations. While this addresses half of the linear range expansion, it does not address the change in the lower concentration regions. Potentially, the improved linear range at low concentrations could be caused by a higher surface-area to volume ratio of the smaller droplet size, allowing more opportunities for extraction. By tuning the droplet size and spacing, the same droptode device can be used for a variety of applications, demonstrating high versatility.

Conclusions

In this paper, we have demonstrated the importance of mixing efficiency and droplet size to droplet efficiency for selective ion sensing. Time on device was shown to not significantly change the droptode response behavior, except in the most extreme cases. However, by increasing mixing, droptodes were shown to have an increased linear range by 1.5 orders of magnitude, as well as a lower limit of detection by an order of magnitude. Increasing the size of the aqueous droplet, compared to the oil phase spacing, was also shown to impact droptode behavior, by increasing the sensitivity of the linear region of the droptode fluorescence response curve. This study suggests that dynamically manipulating flow conditions (aqueous and oil phases) on a single device can result in tunable sensitivities and linear dynamic ranges for ion-selective sensing. Hence, using these approaches may be beneficial in optimizing droptrode responses for a diverse range of analytical measurements of various ionic species via use of different ionophores in the organic phase.

Author Contributions

SPWQ (orcid.org/0000-0003-0614-9212) contributed in project conceptualization, data curation, formal analysis, funding acquisition, investigation, methodology, project administration, validation, visualization and writing. MEM (orcid.org/0000-0002-7841-281X) contributed in project conceptualization and editing. RCB (orcid.org/0000-0003-1021-4267) contributed in project conceptualization, resources, funding acquisition, supervision, reviewing, and editing.

Conflicts of interest

There are no conflicts to declare.

Acknowledgements

S.P.W.Q (DGE-1256260) acknowledges the National Science Foundation for support. The authors would also like to thank Nicolas Mesyngier (University of Michigan) for providing the basis for the MATLAB analysis code.

Notes and references

1 E. Bakker, P. Buhlmann and E. Pretsch. *Chem. Rev*. 1997, **97**, 3083.
2 X. Xie and E. Bakker. *Anal. Bioanal. Chem*. 2017, **407**, 3899.
3 V. Bychkova and A. Sharev. *Anal. Chem*. 2009, **81**, 7416.
4 Q. Zhang, X. Wang, V. Decker, and M.E. Meyerhoff. *ACS Appl. Mater. Interfaces*. 2020, **12**, 25616.
5 Y. Qin and E. Bakker. *Anal. Chem*. 2003, **75**, 6002.
6 X. Wang et al. *Angew. Chemie – Int. Ed*. 2019, **58**, 8092.
7 Y. Xia and G.M. Whitesides. *Angew. Chemie – Int Ed*. 1998, **37**, 550.
8 Y. Ding, P.D. Howes and A.J. Demello. *Anal. Chem*. 2020, **92**, 132.
9 S.R. Doonan, M. Lin, R.C. Bailey. *Lab Chip*. 2019, **19**, 1589.
10 Y. Xu et al. *Lab Chip*. 2018, **18**, 2583.
11 L. Yang, S. Li, J. Liu, and J. Cheng. *Electrophoresis*. 2018, **39**, 512.
12 J. Wang, J. Wang, L. Feng, and T. Lin. *RSC Adv*. 2015, **5**, 104138.
13 V. Menegeaud, J. Josserand, and H.H. Girault. *Anal. Chem*. 2002, **74**, 4279.
14 C.Y. Lee, W.T. Wang, C.C. Liu and L.M. Fu. *Chem. Eng. J.,* 2016, **288**, 146.
15 E. Malinowska and M.E. Meyerhoff. *Anal. Chem*. 1998, **70**, 1477.